Number1 Volume 13 march 2007 Journal of Engineering

FLOW COMPUTATION THROUGH THE PASSAGE BOUNDED BY THE DISH AND SUPPORTS OF THE AWACS

Assist. Prof. Dr. Ihsan Y. Hussien
Mech. Engr. Dept.
College of Engr.
University of Baghdad
Baghdad-Iraq

Shwan F. Mahmood
Mech. Engr. Dept.
College of Engr.
University of Baghdad
Baghdad-Iraq

ABSTRACT

A numerical method has been introduced to predict the flow through a complex geometry bounded by the fuselage, airfoil supports and rotating dish of the AWACS. The finite volume computational approach is used to carry out all computations with staggered grid arrangement. The (k-ε) turbulence model is utilized to describe the turbulent flow. The solution algorithm is based on the technique of automatic numerical grid generation of curvilinear coordinate system having coordinate lines coincident with the boundary counters regardless of its shape. A general coordinate transformation is used to represent complex geometries accurately and the grid is generated using a system of elliptic partial differential equations technique. The extension of the SIMPLE algorithm for compressible flow is used to obtain the required solution.. The results obtained in the present work show that the moving boundary (the rotating dish) has small effects on the free stream and the effects vanish after short distance away from the lower surface of the rotating dish along the span distance. The results of the proposed numerical method show good agreement with available results obtained in literatures.

الخلاصة

تم تقديم طريقة عددية لحساب الجريان خلال المنطقة المعقدة المحاطة بجسم الطائرة، الدعامتين والصحن الدوار لطائرة الانذار المبكر (الاواكس). تم استخدام طريقة الحجوم المحددة لإجراء جميع الحسابات مع العقد الزاحفة. تم استخدام موديل (k-ε) لوصف الجريان المضطرب. اعتمدت خوارزمية الحل على اساس تقنية توليد العقد الذاتية لنظام الاحداثيات المقوس الذي تكون فيه الاحداثيات متطابقة مع حدود الجسم دون الاعتماد على شكله. تم استخدم نظام عام لتحويل الاحداثيات لتمثيل الشكل المعقد بصورة دقيقة وتم تكوين العقد في الشبكة باستخدام تقنية نظام المعادلات التفاضلية الجزئية. طور نظام الخورازمية المعروفة (SIMPLE) للجريان الانضغاطي واستخدم للحصول على الحل المطلوب. أظهرت النتائج المستحصلة ان الصحن الدوار له تأثير قليل على جريان الهواء وأن ذلك التأثير يتلاشي بعد مسافة قصيرة اسفل الصحن باتجاه جسم الطائرة. بينت نتائج الطريقة الحسابية المقترحة توافقا جيداً مع النتائج المستحصلة في البحوث السابقة.

KEY WORDS

AWACS Aerodynamic, Turbulent, Flow, Rotating Dish, Airfoil Dish Supports, Fuselage

INTRODUCTION

Most fluid flow problems in engineering practice have complex boundaries and are subjected to strong variations in the region near solid walls due to the viscous effects. There is an increasing need for powerful methods to calculate the flow processes in such region.

Flow in the region bounded by the rotating dish and its supports and the fuselage of the AWACS, **Fig. (1)**, is extremely complex and is dominated by three dimensional viscous effects that contains viscous, compressible, vortex at the junction of the leading edge and the end walls effects. Therefore it is necessary to investigate the nature of the complex flow running through such a complex passage and get a good understanding of such flow details. Although such information can be obtained by performing experimental measurements, but such obtained results could be very limited, and the range of the running conditions will be relatively narrow. In addition to the fact that the running cost is usually very high. However, the developments in computer technology and advancement achieved in numerical methods have made the computational fluid dynamics (CFD) a very attracting alternative.

Following the recent advances in CFD, the great challenge has been the valuable effort devoted to solve the time averaged dependant Navier-Stokes equations. With further development of computer technology, it has become possible to solve the time dependant Navier-Stokes equations directly with the aid of direct numerical solution (DNS) or large eddy simulation (LES), Wang & Komori (1998), however due to the limitation in both computer storage and memory, at least for present days, both (DNS) and (LES) are practical in solving relatively low Reynolds number flows, otherwise parallel computation methods are required. Nevertheless, the other most popular alternative has always been to solve the time/mass averaged Navier-Stokes (TMANS) equations instead, **Wang & Komori (1998).** The finite volume discrimination, **Patankar (1980**), (based on SIMPLE like algorithm) has been one of the most frequently used methods to solve those (TMANS) equations.

However, important numerical oscillations in pressure field may result due to the introduction of the pressure variation in the continuity equation. In order to avoid such oscillations, the implementation of the extended pressure based method has been carried out in two different ways depending on grid arrangement. For example, **Rieh & Chow (1983)**, **Al-Abbassy (2003)**, adopted non-staggered grid (collocated grid arrangement). On the other hand, **Al-Deroubi (2001)**, **Atta (2000)**, **Karki (1989)**, **Patankar (2000)**, **Gogazeh (2002)** adopted staggered grid arrangement, in this adoption, all primitive variables with exception of velocities are stored at center of control volume while velocity components are stored at the faces of scalar control volume. In both staggered and non staggered implementations, some researchers used grid oriented velocity components (covariant velocity components), while others used Cartesian velocity components as the main dependant variables in the momentum equations. Such a selection depends on the type of the particular problem, and on the way of implementing the proposed solution.

The physical domain related to the present work is the zone bounded by solid boundaries (passage between the elliptical dish, its supports and the fuselage) of the AWACS and the free stream surface as shown in **Fig. (1)**, where it can be seen that this domain consists of four main parts, these are:

1- The frontal zone deliberated in the direction of inlet flow field.
2- The actual space between solid boundaries, where the flow can impact the surface of the rotating dish, airfoil supports and fuselage and divert around them.

3- The rear zone that is far away from the previous zones, where disturbances are decayed and vanished with free stream.
4- The outside zone that represents the free stream envelop surface.

The physical domain considered in the present work is the complex region bounded by the rotating elliptical dish, the supports and the fuselage, which can be summarized by part (2) described above.

As a contribution to the numerical methods of predicting three dimensional flow, the present work is aimed to develop a mathematical model to investigate the flow field passing through the complex region bounded by the fuselage of the airplane, the dish and the two supports of the dish, derive the governing partial differential equation in terms of suitable coordinate system and solve the derived mathematical model by using FDM. A computer code is to be developed and validated to simulate the three dimensional turbulent flow inside the complex zone shown in **Fig. (1)**, (flow bounded by the fuselage and lower dish surface, from one side, and the supports from the other side).

GEOMETRY AND COORDINATE SYSTEMS

The geometry under consideration is shown in **Fig. (2)** consists of interaction of three parts, the first part is two airfoil supports with tapered angle of (87^o) and span distance from fuselage center to dish center of (232 cm). The transverse distance between the two airfoil supports, where they meet the fuselage surface is (83 cm), while it decreases linearly to be (62 cm) at the location where the two supports meet the dish surface. The chord length of the supports is (52.5 cm). The second part is the fuselage, represented by cylindrical surface with a radius of (74 cm) and a length of (1136 cm) from the nose of the airplane to the leading edge of the supports. Finally, the third part is an ellipsoidal rotating dish with a major axis of (222.5 cm) and a minor axis distance of (97 cm). The reference frame of coordinate system is the origin point (0,0,0) located at mid span distance along the center line of the dish. Difficulties associated with the use of Cartesian coordinate systems motivate the introduction of a transformation from physical space (x, y, z) to a generalized curvilinear coordinate space (ξ, η, ζ). The generalized coordinate domain is constructed so that computational boundary in physical space co-insides with coordinate lines in a generalized coordinate space.

GOVERNING PARTIAL DIFFERENTIAL EQUATIONS

The governing equations for the mean velocity and pressure are the mass and momentum equations, these are analyzed utilizing the time/mass averaged Navier-Stokes equations. A calorifically perfect gas is assumed when deriving the energy equation. Finally, a two-equation turbulence model (k-ε) is used for the closure of the system of the momentum equations. In the present work, the working fluid is air and the flow characteristics are assumed to be as follows,

- Steady state flow.
- Fully turbulent flow.
- Compressible effects are significant.
- Newtonian fluid.
- Isentropic with constant specific heat (i.e. perfect gas).

The three dimensional instantaneous governing equations of mass, momentum and energy equation for steady compressible flow can be rewritten in tensor conservation form expressed in Cartesian coordinate system as follows:

- Mass conservative (continuity) equation

$$\frac{\partial}{\partial x_i}\left(\overline{\rho}\tilde{u}_i\right)=0 \tag{1}$$

- Momentum conservative equations

$$\frac{\partial}{\partial x_j}\left(\overline{\rho}\tilde{u}_j\tilde{u}_i\right)=-\frac{\partial \overline{P}}{\partial x_i}+\frac{\partial}{\partial x_j}\left(\overline{\tau_{ij}}+\overline{\mathrm{T}_{ij}}\right)-2\overline{\rho}\left(\omega\times U\right)_i-\overline{\rho}\left[\omega\times\left(\omega\times U\right)\right]_i \tag{2}$$

- Energy equation

$$\frac{\partial}{\partial x_j}\left[\overline{\rho}\tilde{u}_j\tilde{H}\right]=\frac{\partial}{\partial x_j}\left[\tilde{u}_i\left(\overline{\tau_{ij}}+\overline{T_{ij}}\right)\right]+\frac{\partial}{\partial x_j}\left(-\overline{q}_{Lj}-q_{Tj}+\overline{\tau_{ij}u_i''}-\overline{\rho u_i''\frac{1}{2}u_i''u_i''}\right)$$

where $\tilde{H}=C_P\tilde{T}+\frac{1}{2}\left(u_iu_i\right)+\tilde{K}$ (3)

($\overline{T_{ij}}$) is the mass averaged viscous stress tensor represented as,

$$T_{ij}=\left[\mu_e\left(\frac{\partial\tilde{u}_i}{\partial x_j}+\frac{\partial\tilde{u}_j}{\partial x_i}\right)-\frac{2}{3}\left(\frac{\partial\tilde{u}_k}{\partial x_k}\delta_{ij}\right)\right]-\frac{2}{3}\delta_{ij}\overline{\rho}\tilde{k} \tag{4}$$

Here, (q_{Tj}) is the turbulent heat flux vector, usually estimated using simple gradient type-model **(Wang and Komori, 1998).** That is assuming it is proportional to the mean temperature gradient type.

$$q_{Tj}=\overline{\rho u''h''}=-\frac{\mu_TC_P\partial\overline{T}}{\mathrm{Pr}_T\,\partial x_j} \tag{5}$$

where, ($\tilde{k}$) is the mass averaged turbulent kinetic energy, defined as;

$$\tilde{k}=\frac{\overline{\rho\frac{1}{2}u_i''u_i''}}{\overline{\rho}} \tag{6}$$

The turbulent eddy viscosity (μ_T) is expressed to the (k-ε) turbulence model as,

$$\mu_T=\frac{C_\mu\overline{\rho}\tilde{k}^2}{\tilde{\varepsilon}} \tag{7}$$

where ($\overline{\varepsilon}$) is the mass-averaged dissipation rate of turbulence kinetic energy, defined as,

$$\tilde{\varepsilon} = \frac{\overline{\nu\rho\left(\partial u_i'' / \partial x_j\right)\left(\partial u_i'' / \partial x_j\right)}}{\overline{\rho}} \tag{8}$$

- Equation of state

$$\overline{P} = \overline{\rho} R \tilde{T} \tag{9}$$

- Transport equation of turbulence

The standard form of (κ-ε) model can be formulated as follows (**Launder and Spalding, 1972**),

$$\frac{\partial}{\partial x_j}\left(\overline{\rho}\tilde{u}_j\tilde{k}\right) = \frac{\partial}{\partial x_j}\left[\left(\mu + \frac{\mu_T}{\sigma_k}\right)\frac{\partial \tilde{k}}{\partial x_j}\right] + G_k - \overline{\rho}\tilde{\varepsilon} \tag{10}$$

$$\frac{\partial}{\partial x_j}\left(\overline{\rho}\tilde{u}_j\tilde{\varepsilon}\right) = \frac{\partial}{\partial x_j}\left[\left(\mu + \frac{\mu_T}{\sigma_\varepsilon}\right)\frac{\partial \tilde{\varepsilon}}{\partial x_j}\right] + \frac{\tilde{\varepsilon}}{\tilde{k}}\left(C_{\varepsilon 1}G_k - C_{\varepsilon 2}\overline{\rho}\tilde{\varepsilon}\right) \tag{11}$$

where $G_k = \tau_{ij}\dfrac{\partial \tilde{u}}{\partial x_j}$ is the turbulence production term, which is modeled through the following formula (Wang and Komori, 1998),

$$G_k = \mu_T\left(\frac{\partial \tilde{u}_i}{\partial x_k} + \frac{\partial \tilde{u}_k}{\partial x_i}\right)\frac{\partial \tilde{u}_i}{\partial x_k} - \frac{2}{3}\frac{\partial \tilde{u}_j}{\partial x_j}\left(\mu_T\frac{\partial \tilde{u}_\lambda}{\partial x_\lambda} + \rho\tilde{k}\right) \tag{12}$$

In the above equations (C_μ, $C_{\varepsilon 1}$, $C_{\varepsilon 2}$, σ_k and σ_ε) are constants at high Reynolds number and their values are (C_μ = 0..09, $C_{\varepsilon 1}$ = 1.47, $C_{\varepsilon 2}$ = 1.92, σ_k = 1.0 and σ_ε =1.3) **(Launder and Spalding, 1973).**

BOUNDARY CONDITIONS

I. Inlet Boundary:

At inlet, the velocity components (u, v and w), the static pressure, the turbulent kinetic energy (*k*) and its dissipation rate (ε) are specified. The values of (*k* and ε) are approximated based on assumed turbulence intensity (Ti) typically between (1 % and 6 %) and length scale approximation. Approximate values of (*k* and ε) for internal flows can be obtained by means of the following simple assumed forms, **Verstage & Malalasekera (1995)**;

$$k_{in} = \frac{3}{2}\left(u_i.T_i\right)^2 \tag{13}$$

$$\varepsilon_{in} = C_\mu^{3/4}\frac{k^{3/2}}{l}, \quad l = 0.07L \tag{14}$$

where; u_i: inlet velocity

T_i: turbulence intensity.

L: equivalent length

C_μ: universal constant, 0.09

l: length scale of turbulence.

Moult, 1977, assumed that (k and ε) are specified with (k) taken arbitrary as (3%) of the incoming specific kinetic energy and (ε) evaluated with assumed length scale (l) equals (3%) of the domain dimension. It should be noted that the exact proper distribution of flow field can not be specified exactly at inlet because of the irregular shape of inlet boundary, region bounded by lower surface of dish, upper surface of fuselage and leading edge of supports, therefore, it could be determined theoretically by satisfying mass conservation equation.

Let (u_∞) represents free stream velocity, then

$$\dot{m}_{in} = \rho_\infty u_\infty A_{in} \tag{15}$$

To obtain the distribution of inlet boundary condition, it will be assumed that velocity profile of (90 %) of span distance can be obtained by applying the turbulent boundary layer velocity profile,

$$u = u_\infty \left(\frac{y}{\delta}\right)^{1/7} \tag{16a}$$

$$\delta = \frac{0.37x}{\mathrm{Re}^{1/5}} \tag{16b}$$

where (δ) is the boundary layer thickness.

This assumption is quite considerable as the disturbance induced from dish is no longer high as it's compared with free stream velocity, i.e., the angular velocity of dish is so small relative to the free stream velocity. Also, in order to obtain the velocity distribution on the remaining (10 %) of span distance, it will be ensured that the overall continuity equation satisfies the total mass flux on the domain, in other word,

$$\dot{m}_{in} = \dot{m}_{out} \tag{17}$$

$$\left(\rho_\infty u_\infty A_{in}\right) = \sum_{C.V._{in}} \left(\rho_i u^i A^i\right) \tag{18}$$

where, u^i = inlet velocity at node (i).

A^i = area at node (i).

II. Outlet Boundary

Usually the velocity is known only where the fluid enters the physical domain. At outlet the velocity distribution is decided by what happens within the domain **Moult, 1977, Verstage, 1995.** The gradients normal to the outlet surface are assumed to be zero.

III. Wall Boundary

Wall functions are special formula for evaluating effective exchange coefficient at the wall (Γ_{wall}), **Verstage & Malalasetera (1995)**, have summarized the expressions for wall function for different dependent variables based on a dimensionless quantities;

$$y^+ = \frac{\rho \kappa^{1/2} C_D^{1/4} \delta}{\mu_l} \tag{19}$$

$$u^+ = \frac{1}{\kappa} L_n\left(\mathrm{E}.y^+\right) \tag{20}$$

Where (δ) is the distance to the wall from the nearby grid node. The constants (κ and E) come from the law of the wall. Usually (K = 0.4107) and (E = 9.793) for smooth wall, Moult, 1977. In a region very close to the wall, kinetic energy of turbulence is set equal to zero. The value of (ε) is fixed at the near wall point with;

$$\varepsilon = \frac{C_\mu^{3/4} . k^{3/2}}{\kappa . \delta} \tag{21}$$

IV. Moving Boundary

For viscous flow, velocity components normal to the moving boundary (rotating dish) are set to zero while velocity components parallel to the moving boundary are specified.

EQUATIONS IN GENERAL CURVILINEAR COORDINATE SYSTEM

The flow equations in general Cartesian form (x, y, z) are set then transformed into a general curvilinear coordinate system (ξ,η, ζ)

- General conservative form of flow equations

Equations (26, 27, 29 and 13) are all elliptic in nature and can be conveniently presented in general conservative form (parameter).

$$(\rho u \phi)_x + (\rho v \phi)_y + (\rho w \phi)_z = (\Gamma \phi_x)_x + (\Gamma \phi_y)_y + (\Gamma \phi_z)_z + S_{x,y,z} \tag{22}$$

The argument (ϕ) identifies the dependent variable, (Γ) is the exchange coefficient for variable (ϕ) and ($S_{x, y, z}$) is the source term, which can not find a place in equation (30).

DISCRETIZATION OF PARTIAL DIFFERENTIAL EQUATIONS

The governing equations are integrated over each discrete control volume in the computational domain (ξ, η, ζ). A typical control volume with its surrounding neighbor nodes is shown in **Fig. (3)**. The grid arrangement on the physical plane (x-y) and computational plane (ξ-η) are plotted in the corresponding computational plane (ξ-η), which are similar to those shown in **Fig. (3).**

Let's define a new working variable named [$(I\phi)^j$] such that superscript (j) can be any of the computational directions (j = ξ, η, ζ). This is called the total flux in the (j^{th}) direction. It can be shown that;

$$\frac{\partial}{\partial \xi}(I\phi)^\xi + \frac{\partial}{\partial \eta}(I\phi)^\eta + \frac{\partial}{\partial \zeta}(I\phi)^\zeta = SS_{\xi,\eta,\zeta} \tag{23}$$

By integrating equation (23) over the typical control volume node (P) as shown in **Fig. (3b)**, the following result is obtained as follows,

$$\int_b^t \int_s^n \int_w^e \left[\frac{\partial}{\partial \xi}(I\phi)^{\xi} + \frac{\partial}{\partial \eta}(I\phi)^{\eta} + \frac{\partial}{\partial \zeta}(I\phi)^{\zeta} \right] d\xi d\eta d\zeta = \int_b^t \int_s^n \int_w^e SS_{\xi,\eta,\zeta} d\xi d\eta d\zeta \tag{24}$$

For convenience, the above notation can be further simplified as follows,

$$I_e = (I\phi)^{\xi}\Big|_e \Delta\eta\Delta\zeta \tag{25}$$

Using equation (25) and equation (24), it can shown that,

$$I_e - I_w + I_n - I_s + I_t - I_b = SS_{\xi,\eta,\zeta}\Delta V \tag{26}$$

The mass flux at face (e) can be defined as follows,

$$F_e = (\rho G1)_e \Delta\eta\Delta\zeta \tag{27}$$

Therefore,

$$I_e = F_e\phi_E - (\Gamma_1\phi_{\xi})_e \Delta\eta\Delta\zeta \tag{28}$$

At this point, it would be useful to define a quantity (D_e), it is the diffusion term coefficient at face (e). Hence, this coefficient can be expressed as,

$$D_e = \left(\frac{Ja_1\Gamma\Delta\eta\Delta\zeta}{\Delta\xi} \right) \tag{29}$$

Finally, it can be shown that,

$$I_e = F_e\phi_E - D_e(\phi_E - \phi_P) \tag{30}$$

Equation (30) contains the quantity (ϕ_e), which needs to be expressed in terms of neighbor nodal values. This is usually achieved by using an appropriate interpolation scheme. This scheme must be, unconditionally, transportive, conservative and bounded so that the resulting numerical solution is stable and finally converged. Many schemes satisfy the first two criterions, but only the upwinding scheme satisfies all three criterions unconditionally. The implementation of the upwinding scheme is carried out as follows,

$$F_e\phi_e = \phi_P[[F_e,0]] - \phi_e[[-F_e,0]] \tag{31}$$

Hence, the following expression can be obtained,

$$I_e - F_e\phi_P = A_E(\phi_P - \phi_E) \tag{32}$$

Now, recalling the transformed mass conservation equation, which is,

$$(\rho G1)_\xi + (\rho G2)_\eta + (\rho G3)_\zeta = 0 \tag{33}$$

The general discretized form of the conservative general transport equation for property (ϕ) can be written as follows,

$$A_P\phi_P = \sum_{anb} A_{nb}\phi_{nb} + \overline{S}\Delta V \tag{34}$$

Then, by introducing an under relaxation factor (α), the final form of the discretized conservative general transport equation is obtained as follows,

$$\alpha A_P\phi_P = \sum_{anb} A_{nb}\phi_{nb} + \overline{S}\Delta V + (1-\alpha)A_P\phi_P^* \tag{35}$$

where ($0 < \alpha < 1$) and (ϕ_P^*) is the value obtained from previous stage calculation.

CORRECTION OF FLOW FIELD

The momentum equations can be solved only when the pressure field is given or somehow established **(Patankar, 1980)** unless the correct pressure field is employed, the resulting velocity field will not satisfy continuity equation. Our aim in this section is to find a way to improve the guessed pressure such that the resulting velocity field will progressively get closer to satisfy the continuity equation.

VELOCITY CORRECTION

The correction of velocity components are done in two stages,

a) correction of covariant velocity:

Following the SIMPLE algorithm **(Patankar, 1980)**, the correction can be done as shown below: The velocity field obtained from the guessed pressure field will be denoted by (u_ξ^*), (u_η^*) and (u_ζ^*), this "stared" velocity field will result from the solution of the following discretized equations,

$$A_P u_{\xi P}^* = \sum A_{nb}u_{\xi nb}^* - P_\xi^* C_\xi + Su_\xi\Delta V\ ;\ C_\xi = J\Delta V / h_1;\ h_1 = x_\xi^2 + y_\xi^2 + z_\xi^2 \tag{36}$$

The corresponding covariant velocity correction (u_ξ'), (u_η') and (u_ζ') can be introduced in similar manner,

$$u_\xi = u_\xi^* + u_\xi' \tag{37}$$

With reference to the general discritized transport equation (4.31), the descritized momentum equations can be written as follows,

$$A_P u_{\xi P} = \sum A_{nb} u_{\xi_n b} - P_\xi C_\xi + Su_\xi \Delta V$$
$$A_P u_{\eta P} = \sum A_{nb} u_{\eta_n b} - P_\eta C_\eta + Su_\eta \Delta V \quad (38)$$
$$A_P u_{\zeta P} = \sum A_{nb} u_{\zeta_n b} - P_\zeta C_\zeta + Su_\zeta \Delta V$$

The final discretized covariant velocity correction equation becomes,

$$u'_{\xi P} = -P'_\xi C_\xi / A_P = P'_\xi d\xi \quad (39a)$$
$$u'_{\eta P} = -P'_\eta C_\eta / A_P = P'_\eta d\eta \quad (39b)$$
$$u'_{\zeta P} = -P'_\zeta C_\zeta / A_P = P'_\zeta d\zeta \quad (39c)$$

b) Correction of contra-variant velocity

In order to obtain the flow rates that would ensure the conservation of mass, it is preferable to correct the flow rates themselves rather than obtain them from the corrected velocity and density fields (Karki and Patankar, 1989). The major goal is to correct the contra-variant velocity components that are used to calculate the mass flux. The contra-variant velocity components obtained from the guessed pressure field will be denoted by $(G1^*, G2^* \text{ and } G3^*)$.

Similarly, the contra-variant velocity correction $(G1', G2' \text{ and } G3')$ can be expressed as,

$$G1 = G1^* + G1' \quad (40a)$$
$$G2 = G2^* + G2' \quad (40b)$$
$$G3 = G3^* + G3' \quad (40c)$$

By introducing new metrics coefficients (aa, bb, cc, dd, ee, ff, gg, hh and ii) the correction of covariant velocity components becomes,

$$G1' = J\left[P'_\xi d\xi aa + P'_\eta d\eta bb + P'_\zeta d\zeta cc\right] \quad (41a)$$

where,

$$aa = \left(\xi_x^2 + \xi_y^2 + \xi_z^2\right) Jh_1$$
$$bb = \left(\eta_x \xi_x + \eta_y \xi_y + \eta_z \xi_z\right) Jh_2$$
$$cc = \left(\zeta_x \xi_x + \zeta_y \xi_y + \zeta_z \xi_z\right) Jh_3$$

Similarly for $G2' \text{ and } G3'$,

$$G2' = J\left[P'_\xi d\xi dd + P'_\eta d\eta ee + P'_\zeta d\zeta ff\right] \quad (42b)$$

$$dd = \left(\eta_x \xi_x + \eta_y \xi_y + \eta_z \xi_z\right) Jh_1$$
$$ee = \left(\xi_x^2 + \xi_y^2 + \xi_z^2\right) Jh_2$$
$$ff = \left(\zeta_x \eta_x + \zeta_y \eta_y + \zeta_z \eta_z\right) Jh_3$$

$$G3' = J\left[P'_\xi d\xi gg + P'_\eta d\eta hh + P'_\zeta d\zeta ii\right] \quad (43c)$$

$$gg = \left(\xi_x\zeta_x + \xi_y\zeta_y + \xi_z\zeta_z\right) Jh_1$$
$$hh = \left(\zeta_x\eta_x + \zeta_y\eta_y + \zeta_z\eta_z\right) Jh_2$$
$$ii = \left(\zeta_x^2 + \zeta_y^2 + \zeta_z^2\right) Jh_3$$

DENSITY CORRECTION

For compressible flow, the density change becomes significant and it has to be taken into account in the derivation of the mass correction. The corresponding effects will be introduced into the solution of the SIMPLE algorithm. The correction of density is calculated from the following equations **(Karki and Patankar, 1989),**

$$\rho = \rho^* + \rho' \quad (44)$$
$$\rho' = KP' \quad (45)$$

where (ρ^*) is the density obtained from the guessed pressure field and (ρ') is the density correction.

PRESSURE CORRECTION

Solution of the Navier-Stokes equations is complicated by the lack of an independent equation for the pressure, whose gradient contributes to each of the three momentum equations. Furthermore, when the Mach number is low and the flow is incompressible, the continuity equation has no dominant variable **(Ferzigeret et. al., 1999)**. Mass conservation is a kinematic constraint on the velocity field rather than a dynamic equation. One way out of this difficulty is to correct the pressure field to guarantee satisfaction of the continuity equation. Nevertheless, in the case of compressible flow, the continuity equation may be used to determine the density, while the pressure is calculated from the equation of state. However, there are practical mixed types of flows where both zones of compressible and incompressible are usually treated. The (SIMPLE-like algorithm) have been employed by many researchers, and are found to be very applicable in mixed flow problems. The final discritized pressure correction equation can be written in compact form as follows;

$$A_P P'_P = A_E P'_E + A_W P'_W + A_N P'_N + A_S P'_S + A_T P'_T + A_B P'_B + A_{NE} P'_{NE} + A_{SE} P'_{SE} +$$
$$A_{NW} P'_{NW} + A_{SW} P'_{SW} + A_{NB} P'_{NB} + A_{NT} P'_{NT} + A_{SB} P'_{SB} + A_{ST} P'_{ST} + A_{BE} P'_{BE} +$$
$$A_{BW} P'_{BW} + A_{TE} P'_{TE} + A_{TW} P'_{TW} + \dot{m} \quad (46)$$

ALGORITHM SEQUENCE

The algorithm sequence used in the present work can be summarized as follows,

1. Generating computational grid that is suitable for the discretized solution of the three dimensional Navier-Stokes equations.
2. Giving (guessing) the initial values of all variables, while density is calculated from present pressure and temperature fields utilizing the equation of state.
3. The proper boundary conditions are specified for all dependent variables.
4. Solve the discritized momentum equations to obtain the field of covariant velocity components.
5. The pressure correction equation is solved to obtain pressure correction field.

6. Use the obtained pressure corrections to correct the present velocity and pressure fields and correct mass fluxes at the control volume faces. The density fields are corrected using density correction equation.
7. Solve the other dependent scalar variables (i.e. temperature, κ and ε).
8. The whole procedure is repeated from step three until a convergent solution is obtained.

GRID GENERATION

The generation of computational grid that is suitable for the discretized solution of the three dimensional Navier-Stokes equations has always been the subject of intensive researches. This kind of problem covers a wide range of engineering application. This makes it impractical to find a single general gird generation technique that fits the whole range of problems. Therefore, it is rather preferred to employ a suitable technique that is best adapted to the considered type of engineering application.
It is of great importance to implement the surrounding boundaries of arbitrary curvature into PDE and to become apart of the solution itself. The proper choice of the used technique to transform connected region, for example the region surrounding an isolated airfoil, or multiple connected regions, for example the same airfoil with flaps and/or slots is important. The simple connected region can be sub-divided into many simple connected sub-regions to form a multiple connected region. These artificial boundaries between sub-regions are used to smooth and cluster interior grids as desired or even allow to employ grids having different topological structure in different sub-regions.

ELLIPTICAL SURFACE GRID GENERATION

The grid is generated by solving an elliptic system of the form, **Thompson, J. F., et. Al.. 1974**. In analogy with the method of **Thompson, Thames and Mestin (1976),** adopted an equation to obtain the surface grid generation system,

$$g_{\beta\beta}\vec{r}_{\xi^\alpha\xi^\alpha}+g_{\alpha\alpha}\vec{r}_{\xi^\beta\xi^\beta}-2g_{\alpha\beta}\vec{r}_{\xi^\alpha\xi^\beta}+G_v\left(P\vec{r}_{\xi^\alpha}+Q\vec{r}_{\xi^\beta}\right)=\vec{n}^v R^v \tag{47}$$

where P and Q are controlling parameters, α, β and ν are cyclic. We can expand equation (47) to get,

$$g_{22}x_{\xi\xi}+g_{11}x_{\eta\eta}-2g_{12}x_{\xi\eta}+G_\zeta\left(Px_\xi+Qx_\eta\right)=n^\zeta R^\zeta \tag{48a}$$

$$g_{22}y_{\xi\xi}+g_{11}y_{\eta\eta}-2g_{12}y_{\xi\eta}+G_\zeta\left(Py_\xi+Qy_\eta\right)=n^\zeta R^\zeta \tag{48b}$$

THREE DIMENSIONAL GRID GENERATION

Following the method of **Mastin and Thompson (1974),** an elliptic system that can be used to map a three dimensional bounded region out the unit cube in a transformed computational space (ξ, η, ζ) is introduced. The corresponding three dimensional elliptic system can be written as;

$$\alpha_1\left(r_{\xi\xi}+\phi r_\xi\right)+\alpha_2\left(r_{\eta\eta}+\psi r_\eta\right)+\alpha_3\left(r_{\zeta\zeta}+\omega r_\zeta\right)+2\left(\beta_1 r_{\xi\eta}+\beta_2 r_{\eta\zeta}+\beta_3 r_{\xi\zeta}\right)=0 \tag{49}$$

- Face ζ = constant

To obtain the controlling parameter (ϕ and ψ) on the face ζ = constant, two constraints are imposed;

(1) The slope of the transverse grid lines on (ζ) surface is introduced;

$$r_\zeta . r_\xi = \lambda_1$$
$$r_\zeta . r_\eta = \lambda_2 \quad (49)$$

(2) The boundary values come from (ξ, η) surface grid is introduced;

$$r_\xi . r_\eta = \lambda_3 \quad (50)$$

Upon taking the scalar product with (r_ξ and r_η), one obtained pair of linear equations that can be solved easily to obtain unique expressions for evaluating (ϕ and ψ) in terms of the given boundary values at ($\zeta = 1$, $\zeta = N$).

$$\alpha_1\left(r_{\xi\xi} . r_\xi + \phi \left| r_\xi \right|^2 \right) + \alpha_2 \left(r_{\eta\eta} . r_\xi + \psi r_\eta . r_\xi \right) + \alpha_3 \left(r_{\zeta\zeta} . r_\xi + \omega r_\zeta . r_\xi \right) +$$
$$2\left(\lambda_1 r_{\xi\eta} . r_\xi + \lambda_2 r_{\eta\zeta} . r_\xi + \lambda_3 r_{\zeta\xi} . r_\xi \right) = 0 \quad (51a)$$

$$\alpha_1 \left(r_{\xi\xi} . r_\eta + \phi r_\xi . r_\eta \right) + \alpha_2 \left(r_{\eta\eta} . r_\eta + \psi \left| r_\eta \right|^2 \right) + \alpha_3 \left(r_{\zeta\zeta} . r_\eta + \omega r_\zeta . r_\eta \right) +$$
$$2\left(\lambda_1 r_{\xi\eta} . r_\eta + \lambda_2 r_{\eta\zeta} . r_\eta + \lambda_3 r_{\zeta\xi} . r_\eta \right) = 0 \quad (51b)$$

RESULTS

To obtain good predictions for such complex flow field, turbulent models have been introduced. The computations were done for the following conditions;

1. The working fluid is air with constant gas constant (R) and specific pressure (C_P).
2. The velocity and pressure are specified at the inlet of computational domain.
3. The pressure is specified at the exist, while the velocity field is extrapolated at the exist plane.
4. The no slip boundary condition on the solid wall surfaces was imposed.

The main geometry and flow parameters are listed below;
Inlet velocity = 360 Km/hr
Angular velocity of the dish = 3 rpm
Span distance between center of fuselage and center of dish = 232 cm
Chord length of airfoil support = 52.5 cm
Tapered angle of airfoil = 87^o
Distance between airfoil supports measured on fuselage side = 83 cm
Distance between airfoil supports measured on dish side = 62 cm

The velocity vectors and velocity field in passage for (a) 50 %, (b) 75 % (c) 90 % and (d) 95 % of span length are shown in **Fig.** (4 and 5). It can be shown from this figure that the velocity increases downstream due to the convergence of airfoil supports although it is obviously noted that the velocity field increases with span length, whereas the velocity field at 90 % span distance is greater than that at 50 % and 75 % of span distance, this attributes to the tapering shape of the airfoil supports, where the transverse span distance decreases as the distance increases from the fuselage to the dish surface in the

spanwise direction. However, the velocity field at 95 % of span length is of lower value, where effect of the rotating dish is clearly dominant at high span length.

The velocity component normal to the flow direction is shown in **Fig.** (6) for (a) 50 %, (b) 75 % (c) 90 % and (d) 95 % of span length. It can be shown from these figures that a normal velocity to the flow exists no mater how small it is. It is important to mention that the velocity component normal to the flow decreases as moved from the leading edge towards the trailing edge. This is noticed clearly near lower surface of the dish and it can be attributed to elliptical configuration of the dish, where the growth of the boundary layer begins at the leading edge of the dish and increases gradually until it passes over the center of the dish. This zone acts as convergent passage, while the region from the center of the dish towards the trailing edge acts as a divergent passage with possibility of separation at this region, therefore, a negative value of velocity component normal to the flow is located at this zone.

The velocity contours between the dish and the fuselage at the leading edge, mid-chord length and trailing edge is shown in **Fig.** (7). It can be shown that the velocity increases as moved towards the dish in the span distance due to the taper shape of the airfoil supports and then the velocity decreases at high span distance (90 % and 95 %) because of the effect of wall surface of the rotating dish.

The velocity profile at the leading edge, mid-chord length and trailing edge for 50 %, 75 % and 90 % of span distance are shown in **Fig.** (8, 9 and 10). It can be shown from these figures that the velocity increasers as distance in axial direction increases until it reaches its maximum value at the mid of the chord length, region of minimum width, then decreases again due to the divergence of airfoil support trailing edge. Also, it can be shown from these figures that the velocity decreases as moved towards the core until it reaches its minimum value at the center of the core. That is because the velocity decreases in the direction of curvature.

The coefficient of pressure (C_P) in (a) 50 %, (b) 75 % (c) 90 % and (d) 95 % of span length is shown in **Fig.** (11). It can be shown from these figures that the maximum pressure occurs at the beginning of leading edge, where the velocity is stagnant at that point, then decreases until it reaches the tailing edge, where the velocity accelerates again due to the curvature of the airfoil supports and sequentially the pressure increases up again.

The coefficient of pressure (C_P) between the lower surface of the dish and the fuselage is shown in **Fig.** (12). From these figures, it can be shown that at leading edge, pressure decreases as moved inside through the core, where the velocity increases from zero at the wall boundary towards the core, while at the mid chord distance, the pressure increases as moved towards the core, that is because the velocity decreases as moved towards the core.

CONCLUSIONS

Important conclusions can be drawn from this study. These conclusions are:

1- The maximum energy is transformed near the wall between the airfoil supports and the effect of angular velocity of the rotating dish is clearly noticed at 95% of span distance.
2- The kinetic energy and the energy dissipation between the fuselage and the rotating dish are of greater values near wall boundaries and the effect of angular velocity of the rotating dish is noticed on trailing edges.
3- The velocity increases downstream between airfoil supports and in span distance away from the fuselage and it is of lower values at 95% of span distance.

4- A normal velocity component to the flow exists no matter how small it is and it decreases as moved from the leading edge towards the trailing edge. This is clearly noticed near the lower surface of the rotating dish.
5- The maximum pressure occurs at the beginning of leading edge, where the velocity is stagnate at that point, then decreases until it reaches the tailing edge, where the velocity accelerates again.
6- At leading edge, pressure decreases as moved inside through the core, where the velocity increases from zero at the wall boundary towards the core, while at the mid chord distance, the pressure increases as moved towards the core.
7- The wakes and secondary flow occur at the region behind the trailing edge at 95 % span distance, where the velocity field is greater than that at mid span.
8- The moving boundary of the rotating dish has small effects on the axial flow and that the disturbance caused by the rotating dish doesn't propagate to the core region.
9- The effect of angular velocity of dish can be noticed at high span distance near the lower surface of dish.

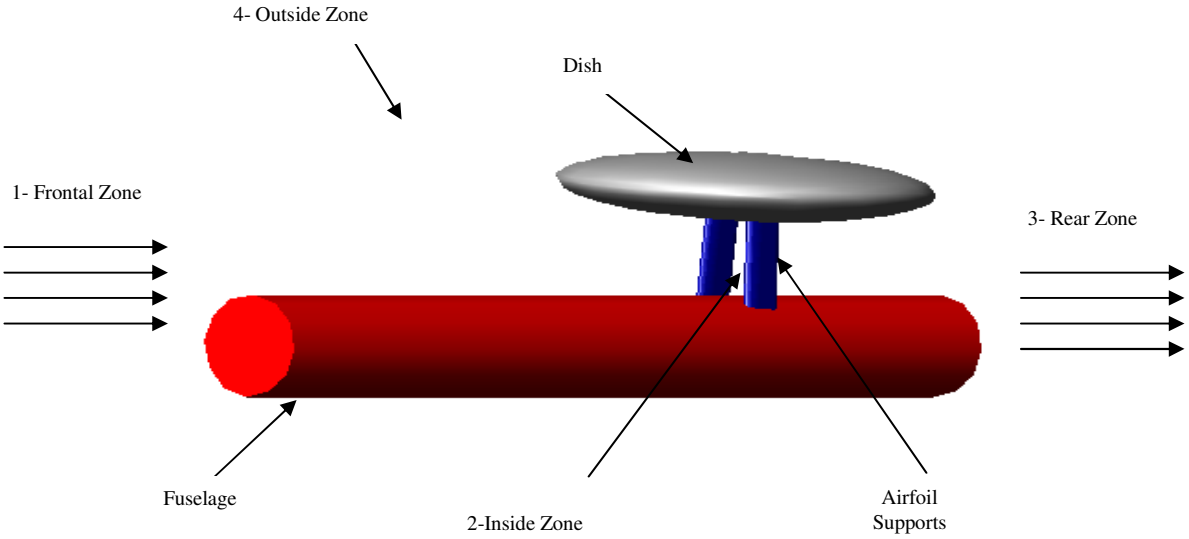

Fig (1): Physical Domains of the Investigated Problem

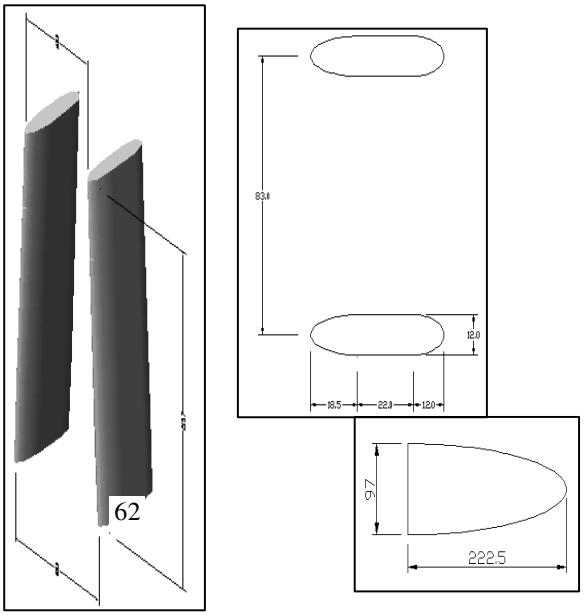

Fig (2): Dimensions for Geometry under Consideration All Dimensions are in cm

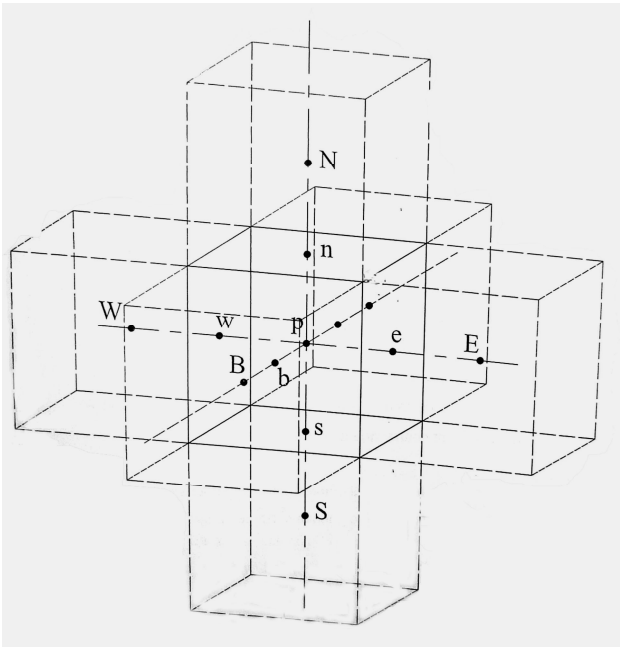

Fig (3) Control Volume Arrangement for General Variable

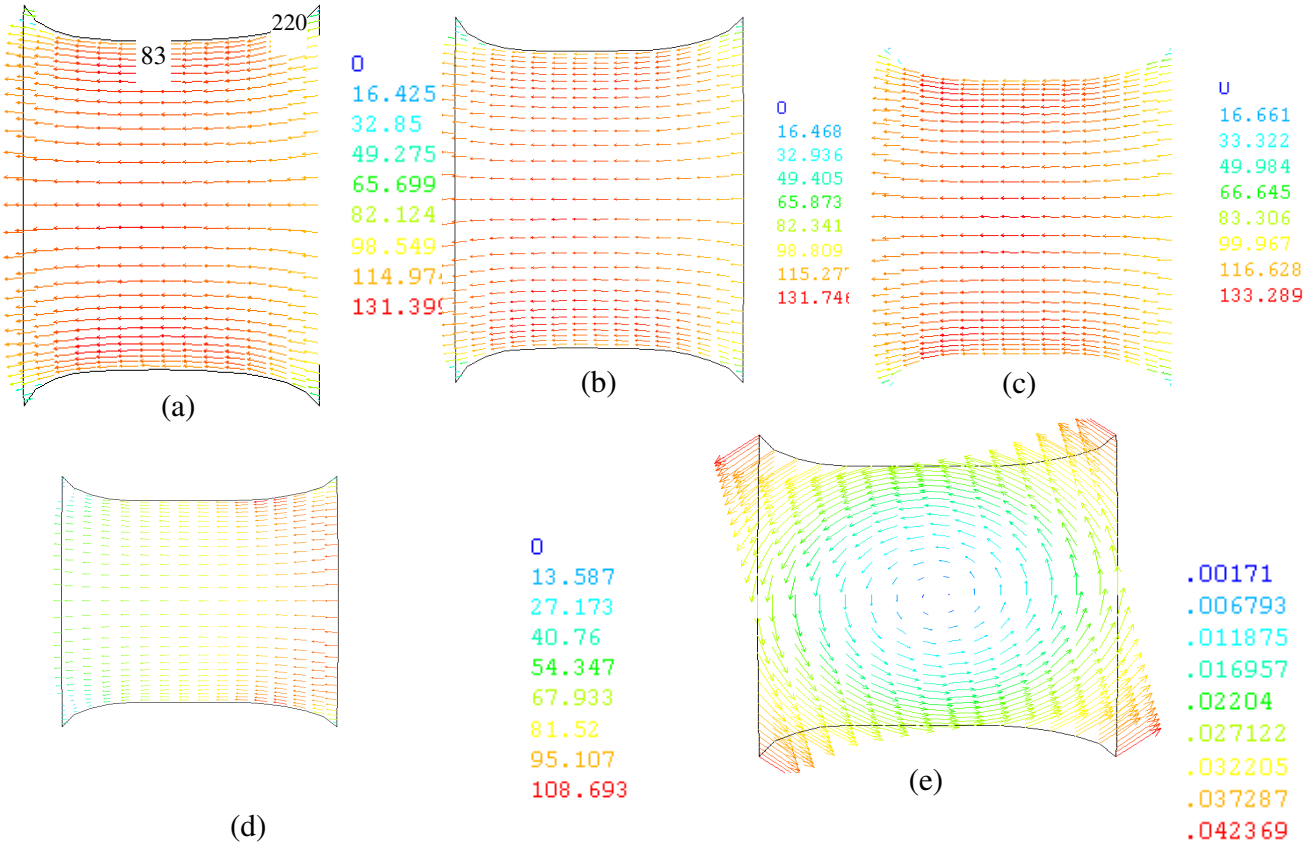

Fig (4): Velocity Vectors between Airfoil Supports
a) 50% of span distance b) 75% of span distance c) 90% of span distance
d) 95% of span distance e) 100% of span distance

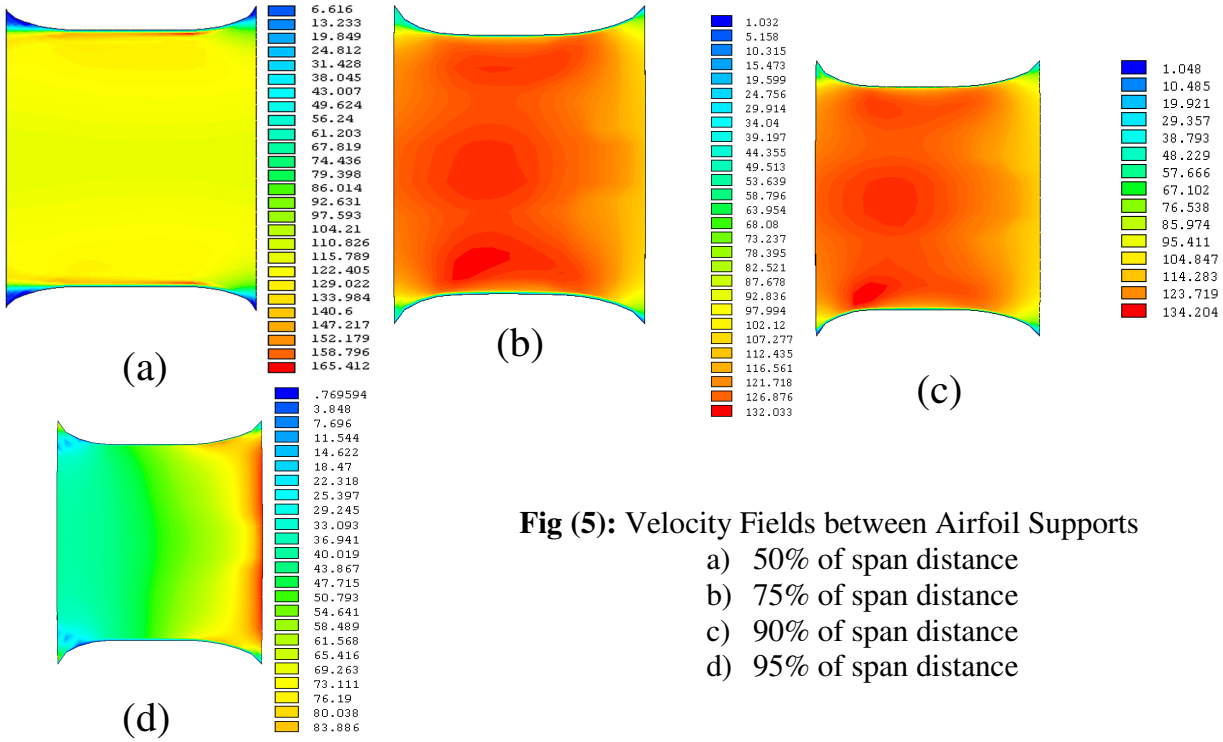

Fig (5): Velocity Fields between Airfoil Supports
a) 50% of span distance
b) 75% of span distance
c) 90% of span distance
d) 95% of span distance

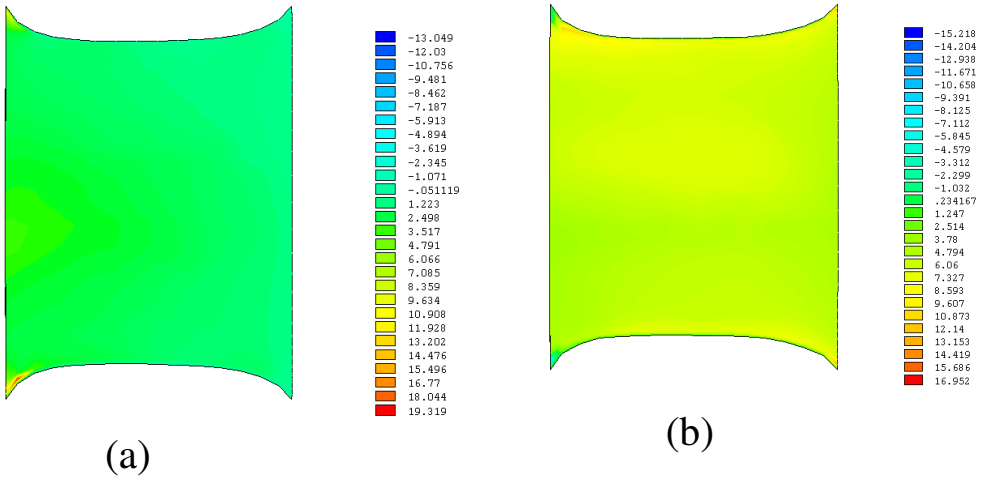

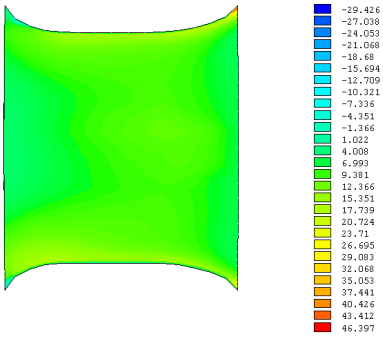

(c)

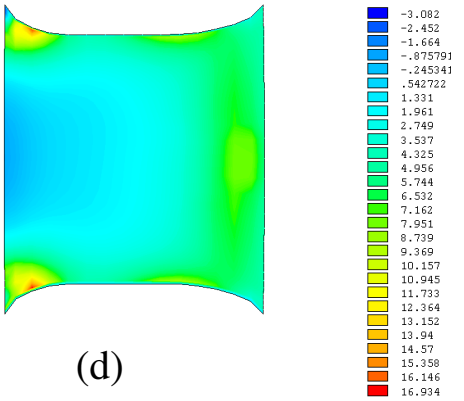

(d)

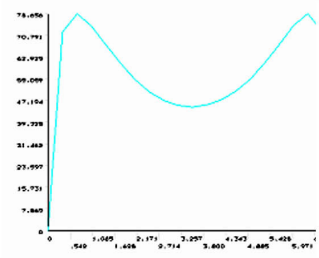

(a)

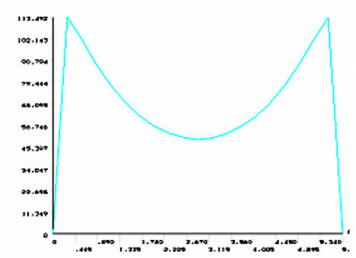

(a)

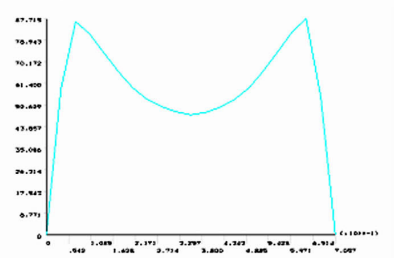

(a)

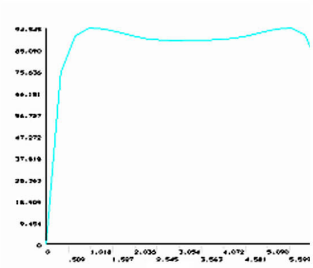

(b)

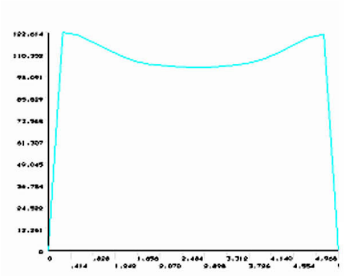

(b)

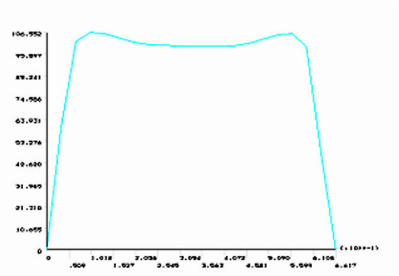

(b)

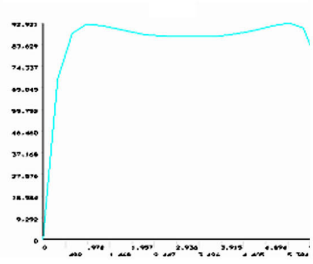

(c)

Velocity Profile at Leading Edge
a) 50% of span distance
b) 75% of span distance
c) 90% of span distance

Fig (8):

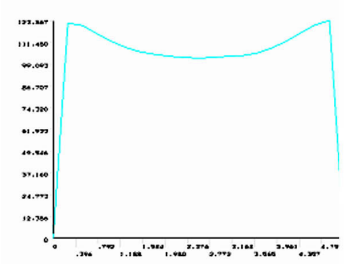

(c)

Velocity Profile at Mid-Chord Len
a) 50% of span distance
b) 75% of span distance
c) 90% of span distance

Fig (9):

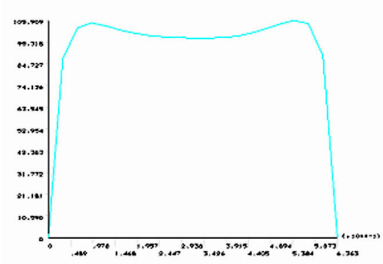

(c)

Velocity Profile at Trailing Edge
a) 50% of span distance
b) 75% of span distance
c) 90% of span distance

Fig (10):

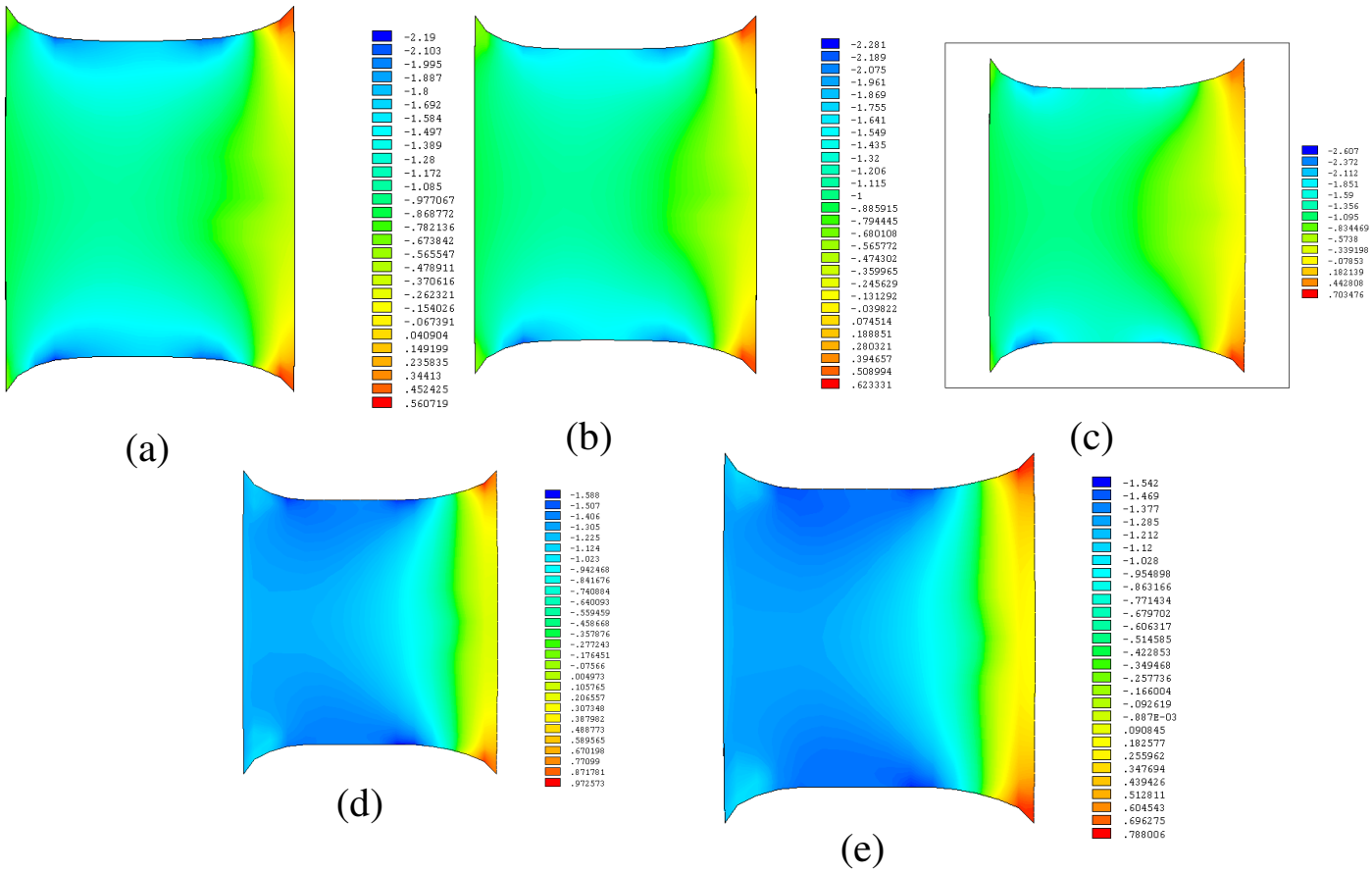

Fig (11): Pressure Coefficient between Airfoil Supports
a) 50% of span distance b) 75% of span distance c) 90% of span distance
d) 95% of span distance e) 100 % of span distance

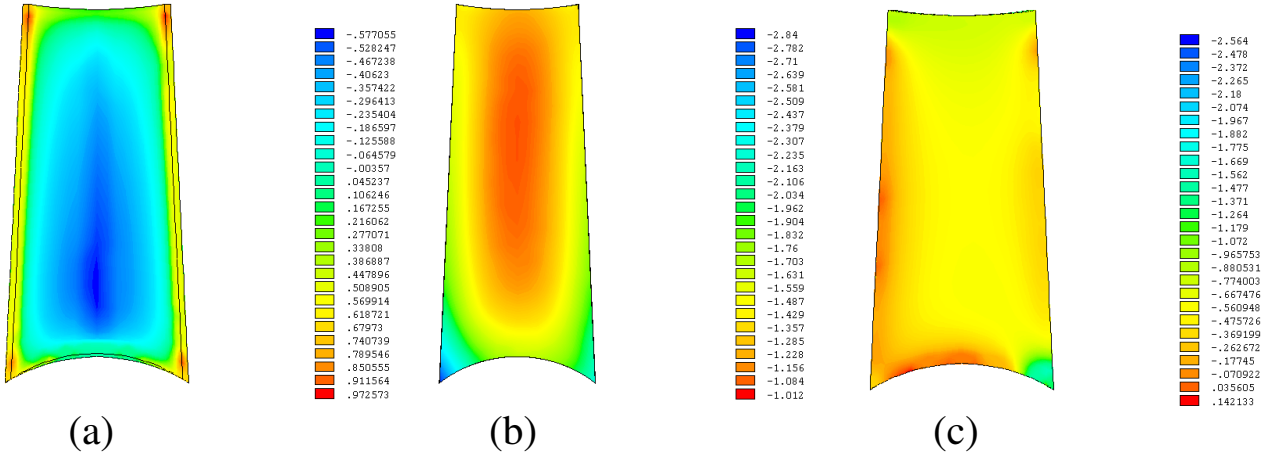

Fig (12): Pressure Coefficient Contour between Dish and Fuselage
a) Leading edge (x/c = 0)
b) Mid chord (x/c = 0.5)
c) Trialing edge (x/c = 1)

REFERENCES

Al-Abbassy, Y. T., 2003: Prediction of the three dimensional compressible turbulent fluid flow inside a gas turbine impeller. Ph. D. Thesis, Mech. Dept. University of Baghdad.

Al-Deroubi, N. N., 2001: Analysis of two dimensional flow between turbomachinery blade using body fitted coordinate system. M. Sc. Thesis, Mech. Dept. University of Baghdad.

Atta, Z. W., 2000: Quasi-three dimensional low speed viscous flow between axial compressor cascade blades. M. Sc. Thesis, Mech. Dept. University of Baghdad.

Ferziger, J. H. and Peric, M, 1999: Computational Methods for Fluid Dynamics, 2nd edition, Springer, Berlin.

Gogezh, M. M., 2000: Three dimensional turbulent flow between two axial compressor blades using body fitted coordinate system. Ph. D. Thesis, Mech. Dept. University of Baghdad.

Karki, K. C. and Patankar, S. V., 1989: Pressure based calculation procedure for viscous flows all speeds in arbitrary configurations. AIAA, J. vol. 27, 1167-1174.

Launder, B.E., and Spalding, D.B., 1973: Mathematical Models of Turbulence, Academic Press, London.

Molt, A. and Srivatsa, S. K., 1977: KORA-2 A computer code for axi-symetrical combustion chambers. Chan computer code 201, London, England.

Patankar, N. A., Singh, P., Joseph, D. D., Glowinski, R. & Pan, T.-W. 2000:
A new formulation of the distributed Lagrange multiplier/fictitious domain method for particulate flows. Int. J. Multiphase Flow **26**, 1509-1524.

Patankar, S. V., 1980: Numerical heat transfer and fluid flow. Hemisphere publishing Corporation, McGraw-Hill Book Co.

Rhie, C. M. and Chow, W. L., 1983: Numerical study of the turbulent flow past an airfoil with trailing edge separation. AIAA J., Vol. 21, no. 11, 1525-1532.

Thompson, J. F., Thames, F. C. and Mastin, C. W., 1974: Automatic numerical generation of body fitted curvilinear coordinate system for field containing any number of arbitrary two dimensional bodies. J. Comp. Phys., vol. 15, 299-319.

Thompson, J. F., Thames, F. C. and Mastin, C. W., 1976: TOMCAT-A code for numerical generation of boundary fitted curvilinear coordinate systems on fields containing any number of arbitrary two dimensional bodies. J. Comp. Phys., vol. 24, 275-302.

Versteeg, H. K. and Malalasekera, W., 1995: An introduction to computational fluid dynamics, the finite volume method. Longman Scientific and technical.

Wang, Y. and Komori, S., (a) 1998: Prediction of duct flows with a pressure base procedure. Numer. Heat Trans., vol. 33, No. 7, 723-748.

Wang, Y. and Komori, S., (a) 1998: Prediction of duct flows with a pressure base procedure. Numer. Heat Trans., vol. 33, No. 7, 723-748.

NOMENCLATURE

$a1,a2,a3$ $b1,b2,b3$	Coordinate transformation coefficient	$1/m^2$
aa,bb,cc,dd	Coefficient in the pressure correction equation	m^3
c	Speed of sound	m/s
c_P	Specific heat	J/kg.^{o}k
$C_\mu, C_{\varepsilon 1}, C_{\varepsilon 2}$	Constants in the k-ε model	
D	Diffusion term	kg/m.s
F	Convection term	kg/m.s
g_{ij}	Metric tensor element	
G_k	Production term of kinetic energy	Pa/s
G_1, G_2, G_3	Contra-variant velocity components	m/s
h	Enthalpy	J/kg
$h1,h,h3$	Geometric quantities	m^2
J	Jacobian of transformation	m^3
J	Determinant of Jacobian of transformation	
k	Turbulent kinetic energy	J
K	$1/c^2$	s^2/m^2
P	Pressure	Pa
P_e	Peclet number	
$\mathrm{Pr}_l, \mathrm{Pr}_t$	laminar, turbulent Prandl number	
q_l, q_t	laminar, turbulent heat flux vector	W
Re	Reynolds number	
S	Source term	
τ_{ij}	Viscous stress tensor	Pascal
T	Temperature	^{o}K
U	Mean velocity	m/s
Ti	Turbulent intensity	
u,v,w	Cartesian velocity components	m/s
u_ξ, u_η, u_ζ	Covariant velocity components	m/s
x,y,z	Cartesian coordinate	m
$y+$	Non-dimensional distance	
α	Under relaxation factor	
θ	Turbulent velocity scale	
K	Thermal conductivity	W/m.oC
ΔV	Volume of control unit	m3
Γ	Diffusion coefficient	
ε	Dissipation rate of turbulent kinetic energy	J/s
κ	Von Karman constant	
μ	Laminar viscosity	Pa.s

μ_T	Turbulent eddy viscosity	Pa.s
μ_e	Effective eddy viscosity	Pa.s
ξ, η, ζ	Curvilinear coordinates	
ρ	Density	kg/m3
$\sigma_\kappa, \sigma_\varepsilon$	Effective Prandtl/Schmidt number	
ν_t	Eddy viscosity	m2/s
τ_{ij}	Reynolds stress tensor	Pa
τ_w	Wall shear stress	Pa
ϕ	Dependent variable	